Low-frequency electric microfield in dense and hot multicomponent plasmas

B. Held
Laboratoire d'Electricité, Université de Pau, Avenue Philippon, F-64000 Pau, France

C. Deutsch and M.-M. Gombert
Laboratoire de Physique des Plasmas, Laboratoire associé au Centre National de la Recherche Scientifique, Université de Paris XI, Bâtiment 212, F-91405 Orsay Cedex, France
(Received 31 May 1983)

The Baranger-Mozer formalism for the computation of low-frequency thermal electric microfield distributions is extended to dense and hot binary ionic mixture relevant to inertial confinement fusion (ICF). The corresponding low-frequency microfield distribution of the thermal electric field, $H(\beta)$, reproduce the Tighe-Hooper results within 0.5%. However, the numerical procedures are more straightforward and shorter. We pay special attention to proportion effects in various Ar^{17+}-H^+ and Ne^{9+}-H^+ mixtures. Particular emphasis is also given to analytic asymptotic distributions valid for $\beta \geq 5$. Extensive numerical results are given in tables and figures.

I. INTRODUCTION

The continuing interest in accurate Stark broadening diagnostics of highly stripped heavy ions immersed in dense and hot plasmas of inertial-confinement-fusion (ICF) study, produced by laser or particle beam drivers, stems largely from the accurate and nondestructive probe of n_e and T_e afforded by a method that also does not require an *a priori* drastic modeling of the plasma thermodynamics.

Keeping in mind diagnostics of current interest[1,2] in this field, we shall devote our concentration in the following paper[3] to Ly-α and Ly-β lines emitted by Ne^{9+} and Ar^{17+} in a dense and hot proton fluid.

As is well known,[4] the ionic plasma component manifests itself in the broadening process through the standard low-frequency microfield distribution of the thermal electric field. It is due to ions screened by the faster moving electrons.[5]

Tighe and Hooper[2] (TH) were the first to design an accurate numerical code providing the corresponding $H(\beta)$ values. Their procedure is based on a rather sophisticated mixture of central and noncentral interactions (as viewed from the emitter charge) which makes the full process quite a long one. Keeping in mind that a different emitter charge requires a new $H(\beta)$, it is easily understood that simpler computational methods yielding results of an accuracy comparable to those of TH are of obvious interest.

In this respect, it is worthwhile to recall that we have recently been able to demonstrate quantitatively[6] that the Baranger-Mozer (BM) scheme reproduces the standard Hooper results[7] for $H(\beta)$ in cold ($T_e \sim$ a few eV) plasmas within 0.5%. The key quantities of numerical interest are the intermediate ones involving the dense plasma corrections through the plasma parameter Λ.

We are thus naturally led to investigate the credibility of the BM cluster expansion for microfield calculations at highly stripped ions in ICF plasmas. Actually, it will be shown in the sequel that the BM approach is again able to reproduce the TH $H(\beta)$ data[3] within 0.5% uncertainty through a much shorter numerical code.

These techniques are especially well suited for plasmas with $\Lambda \leq 1$. However, they also allow us to easily include strong correlation effects ($\Lambda > 1$) through systematic resummations up to infinity of the most important chain diagrams.[8]

In Sec. II, we adapt the BM scheme to a weakly coupled binary ionic mixture (BIM) and detail the essential steps of the $H(\beta)$ calculation. Section III is devoted to mixtures where the proton component is the overwhelming one. A single highly stripped Al component is considered in Sec. IV, while Ar^{17+}-H^+ and Ne^{9+}-H^+ mixtures in any proportions are investigated in Sec. V. Sufficient numerical information is provided in captions and tables.

II. LOW-FREQUENCY MICROFIELDS IN BINARY IONIC MIXTURES (BIM)

In order to save space and prepare the ground for applications of specific ICF interest, we investigate low-frequency distributions $H(\beta)$ in BIM with the aid of the BM cluster expansion for any relative proportions.

A. Notations

Labeling the ions, taken as pointlike, by a (Ne^{9+} or Ar^{17+} for instance) and b (H^+), we introduce the composition parameter

$$p=\frac{C_b}{C_a+C_b}, \quad C_e+C_a+C_b=1 \tag{1}$$

in terms of the relative concentrations $C_{a,b}=N_{a,b}/(N_a+N_b)$. The C's fulfill the neutrality condition

$$-C_e+Z_aC_a+Z_bC_b=0 ,$$

so that

$$C_e=\frac{Z_a+p(Z_b-Z_a)}{\Delta},\quad C_a=\frac{1-p}{\Delta},\quad C_b=\frac{p}{\Delta}\ , \tag{2}$$

where

$$\Delta=(1-p)(Z_a+1)+p(Z_b+1)\ .$$

The corresponding overall BIM screening length ($n=n_i/C_i$, $i=a,b,e$) is read as

$$\lambda_D^2=\frac{\lambda_{D_e}^2}{R^2}\ , \tag{3}$$

in terms of the electron Debye screening length

$$\lambda_{D_e}^2=\frac{k_BT}{4\pi n_e e^2}$$

and

$$R^2=\frac{n}{n_e}(C_e+C_aZ_a^2+C_bZ_b^2)$$
$$=\left[1+\frac{1}{Z_a+p(Z_b-Z_a)}\right]\times\left[1+\frac{(Z_a^2-1)+p(Z_b^2-Z_a^2)}{\Delta}\right]. \tag{4}$$

The dimensionless classical plasma parameter thus reads

$$\Lambda=\frac{e^2}{k_BT\lambda_D}=\frac{\left[1+\dfrac{Z_a^2+p(Z_b^2-Z_a^2)}{Z_a+p(Z_b-Z_a)}\right]^{3/2}}{\left[1+\dfrac{1}{Z_a+p(Z_b-Z_a)}\right]}\Lambda_e\ , \tag{5}$$

with

$$\Lambda_e=\frac{e^2}{k_BT\lambda_{D_e}}=\frac{2\sqrt{2\pi}}{15}V^3=0.334V^3\ , \tag{6}$$

and

$$V=\frac{r_0}{\lambda_{D_e}}=0.0898\frac{n_e^{1/6}\ (\mathrm{cm}^{-3})}{T_e^{1/2}\ (\mathrm{K})}\ , \tag{7}$$

pertaining only to the electron component with r_0 so that $(4/15)(2\pi)^{3/2}n_er_0^3=1$. The Holtsmark unit of field strength thus becomes

$$E_0(\mathrm{kV/cm})\equiv\frac{e}{r_0^2}=3.75\times10^{-10}n_e^{2/3}(\mathrm{cm}^{-3})\ , \tag{8}$$

with the reduced unit $\beta=E/E_0$.

The microfield distributions will be discussed under the usual isotropic form ($u=kE_0$)

$$H(\beta)=\frac{2\beta}{\pi}\int_0^\infty du\ uF(u)\sin(\beta u) \tag{9}$$

in terms of its Fourier transform $F(u)$.

B. Baranger-Mozer formalism

The mathematical quantity of interest is obviously $F(u)$. It is the Fourier transform of the probability $W(\vec{E})$ for finding an electric field

$$\vec{E}=\sum_{j=1}^{N_a}\vec{E}_j^a+\sum_{k=1}^{N_b}\vec{E}_k^b\ , \tag{10}$$

at the origin (emitter) produced by $N=N_a+N_b$ pointlike ions with number densities n_a and n_b. One then gets

$$F(\vec{k})=\int\exp(i\vec{k}\cdot\vec{E})W(\vec{E})d\vec{E}$$
$$=\int\exp(i\vec{k}\cdot\vec{E})p(\vec{r},\vec{r}_2,\ldots,\vec{r}_N)d\vec{r}_1\cdots d\vec{r}_N\ , \tag{11}$$

where $p(\vec{r}_1,\vec{r}_2,\ldots,\vec{r}_N)$ is the joint probability for finding N particles located at $\vec{r}_1,\vec{r}_2,\ldots,\vec{r}_N$.

Upon introducing the auxiliary quantities φ, through

$$\exp(i\vec{k}\cdot\vec{E}_j^a)=1+\varphi_j^a\ ,$$
$$\exp(i\vec{k}\cdot\vec{E}_k^b)=1+\varphi_k^b \tag{12}$$

and making use of Eq. (10) in Eq. (11), $F(\vec{k})$ becomes

$$F(\vec{k})=1+\sum_{(1)}\int p(\vec{r}_j)\varphi_j^a d\vec{r}_j+\sum_{(1)}{}'\int p(\vec{r}_k)\varphi_k^b d\vec{r}_k$$
$$+\sum_{(2)}\int p(\vec{r}_j,\vec{r}_{j'})\varphi_j^a\varphi_{j'}^a d\vec{r}_j d\vec{r}_{j'}$$
$$+\sum_{(2)}{}'\int p(\vec{r}_k,\vec{r}_{k'})\varphi_k^b\varphi_{k'}^b d\vec{r}_k d\vec{r}_{k'}$$
$$+\sum_{(1)}\sum_{(1)}{}'\int p(\vec{r}_j,\vec{r}_k)\varphi_j^a\varphi_k^b d\vec{r}_j d\vec{r}_k+\cdots\ , \tag{13}$$

where $\sum_{(1)}$ ($\sum'_{(1)}$) denotes a sum on ions a (b), while $\sum_{(2)}$ ($\sum'_{(2)}$) is a sum on $aa(bb)$ pairs, and so on. A crucial step in this formalism is the introduction of the cluster expansions

$$V^Mp_M^a(\vec{r}_j,\ldots,\vec{r}_j^M)=\prod_j g_1^a(\vec{r}_j)+\sum_{(2)}g_2^a(\vec{r}_j,\vec{r}_{j'})\prod_{j''}g_1^a(\vec{r}_{j''})+\cdots\ ,$$

$$V^Mp_M^b(\vec{r}_k,\ldots,\vec{r}_k^M)=\prod_k g_1^b(\vec{r}_k)+\sum_{(2)}g_2^b(\vec{r}_k,\vec{r}_{k'})\prod_{k''}g_1^b(\vec{r}_{k''})+\cdots\ , \tag{14}$$

$$V^Mp_M^{ab}(\vec{r}_j,\ldots,\vec{r}_j^M,\vec{r}_k,\ldots,\vec{r}_k^M)=\prod_j g_1^a(\vec{r}_j)\prod_k g_1^b(\vec{r}_k)+\sum_{(2)}g_2^{ab}(\vec{r}_j,\vec{r}_k)\prod_{j'}g_1^a(\vec{r}_{j'})\prod_{k'}g_1^b(\vec{r}_{k'})+\cdots\ ,$$

where M refers to particles located at $\vec{r}_j, \ldots, \vec{r}_j^M$. Correlations appear as systematic corrections to a system of noninteracting ions. Setting Eqs. (14) and (13) yields

$$F(\vec{k})=G_1(\vec{k})G_2(\vec{k})G_3(\vec{k})\cdots , \tag{15}$$

with

$$G_p(\vec{k})=\exp\left[\sum_{q=0}^{p}\frac{n_a^q n_b^{p-q}}{q!(p-q)!}h_{q,p-q}(\vec{k})\right] , \tag{16}$$

and

$$h_{q,p-q}(\vec{k})=\int\cdots\int\varphi_1^a\cdots\varphi_q^a\varphi_{q+1}^b\cdots\varphi_p^b \times g_{p,p-q}(\vec{r}_1,\ldots,\vec{r}_p) \times d\vec{r}_1\cdots d\vec{r}_p , \tag{17}$$

where $g_{p,p-q}$ is the static correlation function for q particles of species a and $p-q$ particles of species b.

Finally, one obtains

$$F(\vec{k})=\exp\left[\sum_{p=1}^{\infty}\sum_{q=0}^{p}\frac{n_a^q n_b^{p-q}}{q!(p-q)!}h_{q,p-q}(\vec{k})\right] . \tag{18}$$

Inverting Eq. (11), the microfield distribution is given as

$$W(\vec{E})=\frac{1}{(2\pi)^3}\int\exp(-i\vec{k}\cdot\vec{E})F(\vec{k})d\vec{k} , \tag{19}$$

with ions a and b treated exactly on the same footing. Upon introducing the dimensionless $u=kE_0$, and taking the angular average in Eq. (19), one retrieves Eq. (9) with Eq. (18).

For most cases of practical interest,[1,2] we shall restrict ourselves to weakly coupled systems ($\Lambda\leq 1$). Equation (18) may then be stopped at order Λ^2 with

$$F(u)\simeq\exp[n_a h_1^a(u)+n_b h_1^b(u)+n_a n_b h_2^{ab}(u) +\tfrac{1}{2}n_a^2 h_2^a(u)+\tfrac{1}{2}n_b^2 h_2^b(u)] \tag{20}$$

and

$$\begin{aligned} h_1^a(u)&=\int_{(1)}\varphi_1^a g_1^a(\vec{r}_1)d\vec{r}_1 ,\\ h_2^a(u)&=\int_{(1)}\int_{(2)}\varphi_1^a\varphi_2^a g_2^a(\vec{r}_1,\vec{r}_2)d\vec{r}_1 d\vec{r}_2 ,\\ h_1^b(u)&=\int_{(1)}\varphi_1^b g_1^b(\vec{r}_1)d\vec{r}_1 ,\\ h_2^b(u)&=\int_{(1)}\int_{(2)}\varphi_1^b\varphi_2^b g_2^b(\vec{r}_1,\vec{r}_2)d\vec{r}_1 d\vec{r}_2 ,\\ h_2^{ab}(u)&=\int_{(1)}\int_{(2)}\varphi_1^a\varphi_2^b g_2^{ab}(\vec{r}_1,\vec{r}_2)d\vec{r}_1 d\vec{r}_2 , \end{aligned} \tag{21}$$

where $\vec{r}_1$ ($\vec{r}_2$) denotes location of ion a (b), and the correlations functions[8] g_1^a, g_2^a, g_1^b, g_2^b, g_2^{ab} detailed in the sequel.

Making use of a spherical harmonics expansion

$$\varphi_i^{a,b}=\sum_l i^l[4\pi(2l+1)]^{1/2}[j_l(Z_i^{a,b})-\delta_{l_0}]Y_{l_0}(\theta_i,\omega_i) , \tag{22}$$

where $j_l(Z)$ is a spherical Bessel function, the h_1's are expressed as ($Z_i^{a,b}=kE_i^{a,b}$, $X_i=r_i/\lambda_{D_e}$)

$$n_a h_1^{a,b}(u)=-u^{3/2}\psi_1^{a,b}(a) , \tag{23}$$

$$\psi_1^{a,b}(a)=\frac{15}{2(2\pi)^{1/2}}\frac{n_{a,b}}{n_e}\frac{1}{a^3} \times\int_0^\infty[1-j_0(Z_1^{a,b})]g_1^{a,b}(X_1)X_1^2dX_1 , \tag{24}$$

where the argument $a=u^{1/2}v=\sqrt{ke}/\lambda_{D_e}$ is not to be confused with the upper index labelings of the heavy-ion component.

Similarly one gets

$$\begin{aligned} h_{2,\Lambda}^a(u)&=\Lambda\lambda_{D_e}^6\int_{(1)}\int_{(2)}\varphi_1^a\varphi_2^a g_{2,\Lambda}^a(X)d\vec{X}_1 d\vec{X}_2 ,\\ h_{2,\Lambda}^b(u)&=\Lambda\lambda_{D_e}^6\int_{(1)}\int_{(2)}\varphi_1^b\varphi_2^b g_{2,\Lambda}^b(X)d\vec{X}_1 d\vec{X}_2 ,\\ h_{2,\Lambda}^{ab}(u)&=\Lambda\lambda_{D_e}^6\int_{(1)}\int_{(2)}\varphi_1^a\varphi_2^b g_{2,\Lambda}^{ab}(X)d\vec{X}_1 d\vec{X}_2 \end{aligned} \tag{25}$$

in terms of the first-order part of the static correlations, under the form

$$\begin{aligned} \tfrac{1}{2}n_a^2 h_{2,\Lambda}^a(u)&=u^{3/2}\psi_{2,\Lambda}^a(a) ,\\ \tfrac{1}{2}n_b^2 h_{2,\Lambda}^b(u)&=u^{3/2}\psi_{2,\Lambda}^b(a) ,\\ n_a n_b h_{2,\Lambda}^{ab}(u)&=u^{3/2}\psi_{2,\Lambda}^{ab}(a) , \end{aligned} \tag{26}$$

where $\psi_{2,\Lambda}^a(a)$, $\psi_{2,\Lambda}^b(a)$, and $\psi_{2,\Lambda}^{ab}(a)$ are given by

$$\begin{aligned} \psi_{2,\Lambda}^a(a)&=\frac{15}{2(2\pi)^{1/2}}\left[\frac{n_a}{n_e}\right]^2\frac{1}{a^3}\sum_i\alpha_{\Lambda,i}^a W_{\Lambda,i}^a(a) ,\\ \psi_{2,\Lambda}^b(a)&=\frac{15}{2(2\pi)^{1/2}}\left[\frac{n_b}{n_e}\right]^2\frac{1}{a^3}\sum_i\alpha_{\Lambda,i}^b W_{\Lambda,i}^b(a) ,\\ \psi_{2,\Lambda}^{ab}(a)&=\frac{15}{2(2\pi)^{1/2}}\left[\frac{2n_a n_b}{n_e^2}\right]\frac{1}{a^3}\sum_i\alpha_{\Lambda,i}^{ab} W_{\Lambda,i}^{ab}(a) , \end{aligned} \tag{27}$$

with

$$\begin{aligned} W_{\Lambda,i}^a(a)&=\sum_l(-1)^l(2l+1)\chi_{\Lambda,i}^{l,a}(a) ,\\ W_{\Lambda,i}^b(a)&=\sum_l(-1)(2l+1)\chi_{\Lambda,i}^{l,b}(a) ,\\ W_{\Lambda,i}^{ab}(a)&=\sum_l(-1)(2l+1)\chi_{\Lambda,i}^{l,ab}(a) \end{aligned} \tag{28}$$

and

$$\begin{aligned} \chi_{\Lambda,i}^{l,a}(a)&=\int_0^\infty\int_0^{X_1}[j_l(Z_1^a)-\delta_{l_0}][j_l(Z_2^a)-\delta_{l_0}]\frac{f_{\Lambda,i}^{l,a}}{4\pi}X_1^2X_2^2dX_1dX_2 ,\\ \chi_{\Lambda,i}^{l,b}(a)&=\int_0^\infty\int_0^{X_1}[j_l(Z_1^b)-\delta_{l_0}][j_l(Z_2^b)-\delta_{l_0}]\frac{f_{\Lambda,i}^{l,b}}{4\pi}X_1^2X_2^2dX_1dX_2 ,\\ \chi_{\Lambda,i}^{l,ab}(a)&=\tfrac{1}{2}\int_0^\infty\int_0^{X_1}\{[j_{l_1}(Z_1^a)-\delta_{l_0}][j_l(Z_2^b)-\delta_{l_0}]+[j_l(Z_2^a)-\delta_{l_0}][j_l(Z_1^b)-\delta_{l_0}]\}\frac{f_{\Lambda,i}^{l,ab}}{4\pi}X_1^2X_2^2dX_1dX_2 . \end{aligned} \tag{29}$$

The $\alpha^j_{\Lambda,i}$ [Eq. (27)] will be specified later on, while $f^{l,j}_{\Lambda,i}$ comes out from the spherical expansion ($j=a,b,ab$)

$$\phi^f_{\Lambda,i}=\sum_l \sum_{m=-l}^{+l} f^{l,j}_{\Lambda,i}(X_1,X_2)Y^*_{lm}(\theta_1,\omega_1)Y_{lm}(\theta_2,\omega_2) , \tag{30}$$

for the Λ part of g^j_2.

The central quantity $F(u)$ is then well approximated by

$$F(u)\simeq\exp[F^{(1)}(u)+F^{(2)}(u)] , \tag{31}$$

with

$$\begin{aligned}F^{(1)}(u)&=n_a h^a_1(u)+n_b h^b_1(u)\\ &=-u^{3/2}[\psi^a_1(a)+\psi^b_1(a)]\end{aligned} \tag{32}$$

and

$$\begin{aligned}F^{(2)}(u)&=\tfrac{1}{2}n_a^2h_a^2(u)+\tfrac{1}{2}n_b^2h^b_2(u)+n_a n_b h^{ab}_2(u)\\ &=u^{3/2}[\psi^a_{2,\Lambda}(a)+\psi^b_{2,\Lambda}(a)+\psi^{ab}_{2,\Lambda}(a)] .\end{aligned} \tag{33}$$

It can be computed for any mixture through the ψ's and taking into account ions screened by electrons with ($j=a,b$)

$$\vec{\mathrm{E}}^j_i=-Z_j e\left[1+\frac{r_i}{\lambda_{D_e}}\right]e^{-r_i/\lambda_{D_e}}\frac{\vec{\mathrm{r}}_i}{r_i^3} , \tag{34}$$

and the $Z_i^{a,b}$ [Eq. (22)] given as ($j=a,b$)

$$Z^j_i=Z_j\frac{a^2}{X_i^2}(1+X_i)e^{-X_i} . \tag{35}$$

The usual one-component-plasma (OCP) low frequency $H(\beta)$ is easily recovered through

$$\begin{aligned}n_a&=\frac{1-p}{Z_a+p(Z_b-Z_a)}n_e ,\\ n_b&=\frac{p}{Z_a+p(Z_b-Z_a)}n_e ,\end{aligned} \tag{36}$$

from Eq. (31) which becomes

$$F(u)=\exp\left[\frac{n_e}{[Z_a+p(Z_b-Z_a)]}[(1-p)h^a_1(u)+ph^b_1(u)] + \frac{1}{2}\frac{n_e^2}{[Z_a+p(Z_b-Z_a)]^2}[(1-p)^2h^a_2(u)+2p(1-p)h^{ab}_2(u)+p^2h^b_2(u)]\right] . \tag{37}$$

A pure proton phase ($p=1$) is obtained by setting $Z_a=Z_b=1$ in the above, which reduces to

$$F(u)=\exp[n_e h^a_1(u)+\tfrac{1}{2}n_e^2h^a_2(u)] , \tag{38}$$

with [Eq. (4)] $R^2=2$.

III. HIGH-Z IMPURITIES IN DENSE PROTONS ($p\simeq1$)

Here we allude to the possibility of using small traces of highly stripped ions (currently Ne^{9+} or Ar^{17+}) in a proton or deuterium fill, as a probe of the plasma parameters through Stark broadening. The low-frequency distribution is thus taken on a heavy ion (a). Equations (32) and (33) now read (first order in Λ)

$$\begin{aligned}&n_a h^a_1(u)+n_b h^b_1(u)=-u^{3/2}\psi^b_c(a) ,\\ &\tfrac{1}{2}n_a^2h^a_2(u)+\tfrac{1}{2}n_b^2h^b_2(u)+n_a n_b h^{ab}_2(u)=u^{3/2}\psi^b_{2,\Lambda}(a) .\end{aligned} \tag{39}$$

Heavy ions a appear only in the first line with $\psi^b_a(a)$ taking into account the a-b interaction through the two-point distribution

$$g_2(X)=\exp\left[-Z_aZ_b\frac{e^{-RX}}{X}\right]-1 , \tag{40}$$

The second line of Eq. (39) retains only b-b (within protons) with

$$g_2(X)=\exp\left[-Z_b^2\Lambda\frac{e^{-RX}}{X}\right]-1 . \tag{41}$$

Introducing Eq. (40) into Eq. (24) yields

$$\begin{aligned}\psi^b_c(a)&=\frac{15}{2(2\pi)^{1/2}}\frac{1}{a^3}\\ &\times\int_0^\infty[1-j_0(Z^b_1)]\exp\left[-Z_aZ_b\frac{e^{-RX_1}}{X_1}\right]X_1^2dX_1 ,\\ Z^b_1&=\frac{a^2}{X_1^2}(1+X_1)e^{-X_1} ,\\ R^2&=2 ,\end{aligned} \tag{42}$$

where ($p=1$, $Z_b=1$). Equations (42) are plotted, respectively, in Figs. 1 and 2 for Ar^{17+} and Ne^{9+}. The second line of Eq. (39) is identical to the corresponding OCP quantity.[6]

Therefore $\psi^b_{2,\Lambda}(a)$ and $\psi^b_{2,\Lambda^2}(a)$ are, respectively, identical to $\psi_{2,\Lambda}(a)$ and $\psi_{2,\Lambda^2}(a)$ already worked out in Ref. 6.

It then suffices to replace $\psi^b_{2,\Lambda}(a)$ by $(\psi_{2,\Lambda}+v^3\psi_{2,\Lambda^2})$ in the right-hand side (rhs) of the second line of Eq. (39), to retain static correlations up to Λ^2. Finally, the low-frequency component at Z_a,

$$H(\beta)=\frac{2\beta}{\pi}\int_0^\infty uF(u)\sin(\beta u)du , \tag{43}$$

with

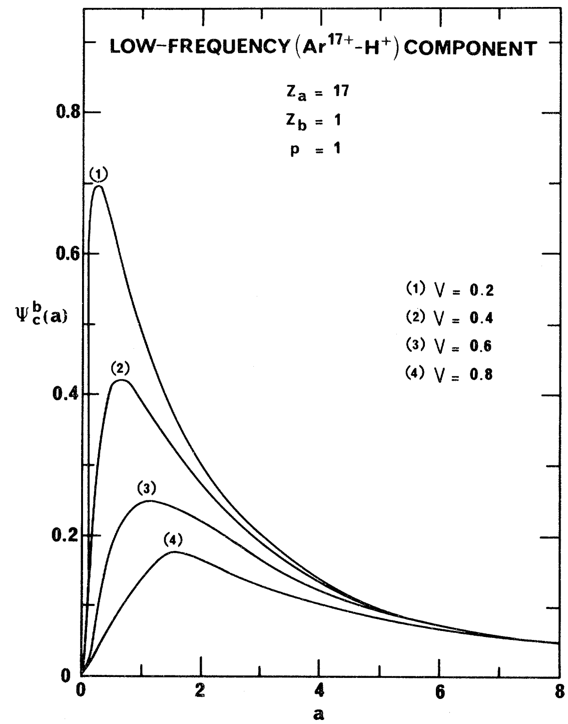

FIG. 1. $\psi_c^b(a)$ [Eq. (42)] plotted for an Ar^{17+}-H^+ mixture.

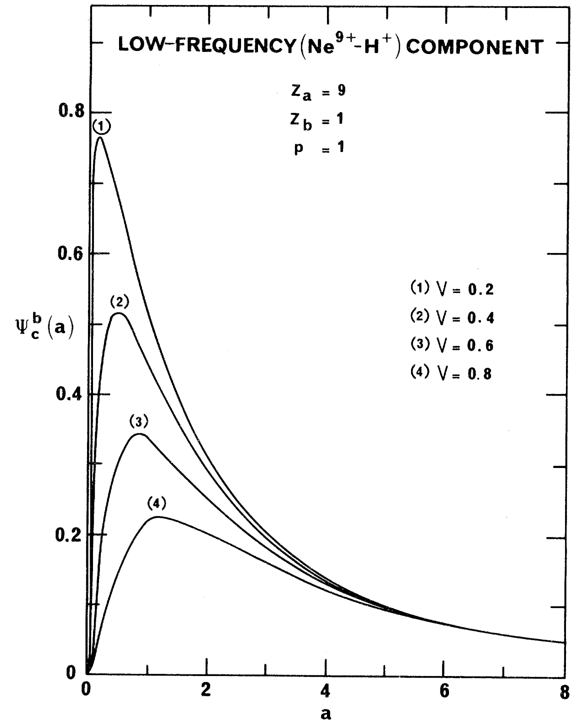

FIG. 2. $\psi_c^b(a)$ [Eq. (42)] plotted for a Ne^{9+}-H^+ mixture.

$$F(u)=\exp\{-u^{3/2}[\psi_c^b(a)-\psi_{2,\Lambda}(a)-v^3\psi_{2,\Lambda^2}(a)]\} , \quad (44)$$

is given numerically in Tables I and II and pictured in Figs. 3 and 4. It should be mentioned that the present calculations are limited up to $\beta \leq 5$. The $\beta > 5$ data are obtained by asymptotic techniques worked out in Sec. V.

IV. HEAVY-ION COMPONENT ALONE ($p=0$)

A particularly important application of the general formalism worked out in Sec. II concerns the highly stripped ion component a alone. The corresponding plasma model is of a special relevance to the outer layers (high Z) of targets designed for heavy-ion fusion.[9,10] As a working example, let us consider $Z_a=10$ with $p=0$. $H(\beta)$ is then deduced from Eq. (32) written as

$$n_a h_1^a(u)+n_b h_1^b(u)=-u^{3/2}\psi_c^a(a) , \quad (45)$$

with

$$\psi_c^a(a)=\frac{15}{2(2\pi)^{1/2}}\frac{1}{z_a}\frac{1}{a^3} \times\int_0^\infty[1-j_0(Z_1^a)] \times\exp\left[-Z_a^2\Lambda\frac{e^{-RX_1}}{X_1}\right]X_1^2dX_1 . \quad (46)$$

In order to implement Eq. (33), it should be recalled that the a-a interaction is now a strongly coupled one which does not allow any more the linearization of the static pair correlations

$$g_2(X)=\exp\left[-Z_a^2\Lambda\frac{e^{-RX}}{X}\right] . \quad (47)$$

Hopefully,[8] a Debye-type $g_2(X)$ may be recovered by resumming the longest chain diagrams up to infinity, under the form

$$g_2(X)=-Z_a^2\Lambda\frac{e^{-R'X}}{X} , \quad (48)$$

where

$$R'=\tfrac{1}{8}\left[\frac{17}{2}+\frac{2(2\pi)^{1/2}}{15}Z_a^2V^3R\right]R .$$

Equation (33) thus reads

$$\tfrac{1}{2}n_a^2h_2^a(u)+\tfrac{1}{2}n_b^2h_2^b(u)+n_an_bh_2^{ab}(u)=u^{3/2}\psi_{2,\Lambda}^a(a) , \quad (49)$$

with $\psi_{2,\Lambda}^a(a)$ already computed in Ref. 6. The numerical $H(\beta)$ data (Table III and Fig. 5) are obtained through

$$F(u)=\exp\{-u^{3/2}[\psi_c^a(a)-\psi_{2,\Lambda}^a(a)]\} . \quad (50)$$

V. Ne^{9+}-H^+ IN ANY PROPORTIONS

Moving to the general case of a BIM with any p, Eqs. (32) and (33) now take the following form: For $p=0.0$

$$n_ah_1^a(u)+n_bh_1^b(u)=-u^{3/2}\psi_1^a(a) ,$$

$$\tfrac{1}{2}n_a^2h_2^a(u)+\tfrac{1}{2}n_b^2h_2^b(u)+n_an_bh_2^{ab}(u)=u^{3/2}\psi_{2,\Lambda}^a(a) ,$$

for $p=0.5$

TABLE I. Low-frequency microfield distribution at an ion Ar^{17+} immersed in a dense proton plasma ($p \cong 1$).

β	V 0.2	0.4	0.6	0.8
0.1	0.96128×10^{-2}	0.27887×10^{-1}	0.72291×10^{-1}	0.16475
0.2	0.37499×10^{-1}	0.10614	0.26359	0.55577
0.3	0.80938×10^{-1}	0.22009	0.51066	0.95757
0.4	0.13584	0.34982	0.74284	0.12135×10^{1}
0.5	0.19728	0.47510	0.90905	0.12829×10^{1}
0.6	0.26016	0.57962	0.98859	0.12111×10^{1}
0.7	0.31978	0.65338	0.98691	0.10614×10^{1}
0.8	0.37227	0.69298	0.92422	0.88338
0.9	0.41488	0.70046	0.82474	0.70734
1.0	0.44607	0.68135	0.70968	0.54937
1.1	0.46542	0.64268	0.59433	0.41630
1.2	0.47347	0.59153	0.48798	0.30917
1.3	0.47139	0.53399	0.39512	0.22579
1.4	0.46082	0.47484	0.31697	0.16266
1.5	0.44355	0.41740	0.25286	0.11594
1.6	0.42137	0.36380	0.20115	0.82003×10^{-1}
1.7	0.39594	0.31518	0.15992	0.57630×10^{-1}
1.8	0.36867	0.27198	0.12728	0.40238×10^{-1}
1.9	0.34073	0.23416	0.10151	0.27878×10^{-1}
2.0	0.31303	0.20142	0.81208×10^{-1}	0.19097×10^{-1}
2.5	0.19568	0.97609×10^{-1}	0.28794×10^{-1}	0.67632×10^{-2}
3.0	0.11919	0.49319×10^{-1}	0.12800×10^{-1}	0.24110×10^{-2}
3.5	0.75145×10^{-1}	0.27183×10^{-1}	0.65287×10^{-2}	0.97685×10^{-3}
4.0	0.49489×10^{-1}	0.16095×10^{-1}	0.35063×10^{-2}	0.44142×10^{-3}
4.5	0.34035×10^{-1}	0.10147×10^{-1}	0.20748×10^{-2}	0.20748×10^{-3}
5.0	0.24332×10^{-1}	0.672995×10^{-2}	0.11956×10^{-2}	0.11287×10^{-3}
6.0	0.13629×10^{-1}	0.32603×10^{-2}	0.47821×10^{-3}	0.35861×10^{-4}
7.0	0.83864×10^{-2}	0.17177×10^{-2}	0.21740×10^{-3}	0.13717×10^{-4}
8.0	0.55221×10^{-2}	0.10167×10^{-2}	0.10771×10^{-3}	0.55243×10^{-5}
9.0	0.38254×10^{-2}	0.66888×10^{-3}	0.54877×10^{-4}	0.25965×10^{-5}
10.0	0.27561×10^{-2}	0.43071×10^{-3}	0.29991×10^{-4}	0.11695×10^{-5}
12.0	0.15618×10^{-2}	0.18974×10^{-3}	0.10927×10^{-4}	0.27291×10^{-6}
14.0	0.96319×10^{-3}	0.10869×10^{-3}	0.43137×10^{-5}	0.70180×10^{-7}
16.0	0.62632×10^{-3}	0.60085×10^{-4}	0.18539×10^{-5}	0.21764×10^{-7}
18.0	0.44493×10^{-3}	0.36261×10^{-4}	0.85863×10^{-6}	0.69563×10^{-8}
20.0	0.31690×10^{-3}	0.22694×10^{-4}	0.41678×10^{-6}	0.23629×10^{-8}
22.0	0.24019×10^{-3}	0.14919×10^{-4}	0.20252×10^{-6}	0.88381×10^{-9}
24.0	0.18467×10^{-3}	0.99711×10^{-5}	0.10692×10^{-6}	0.33857×10^{-9}
26.0	0.14448×10^{-3}	0.68131×10^{-5}	0.58141×10^{-7}	0.13494×10^{-9}
28.0	0.11540×10^{-3}	0.47883×10^{-5}	0.32922×10^{-7}	0.56926×10^{-10}
30.0	0.94418×10^{-4}	0.32983×10^{-5}	0.19634×10^{-7}	0.25895×10^{-10}
35.0	0.57228×10^{-4}	0.15533×10^{-5}	0.57594×10^{-8}	0.33783×10^{-11}
40.0	0.37226×10^{-4}	0.76406×10^{-6}	0.17844×10^{-8}	0.54057×10^{-12}
45.0	0.25456×10^{-4}	0.40307×10^{-6}	0.61258×10^{-9}	0.12202×10^{-12}
50.0	0.17717×10^{-4}	0.21661×10^{-6}	0.21450×10^{-9}	0.23576×10^{-13}
60.0	0.97764×10^{-5}	0.76345×10^{-7}	0.35956×10^{-10}	0.14073×10^{-14}
70.0	0.59674×10^{-5}	0.28248×10^{-7}	0.63806×10^{-11}	0.89873×10^{-16}
80.0	0.36919×10^{-5}	0.12954×10^{-7}	0.16172×10^{-11}	0.99780×10^{-17}
90.0	0.23355×10^{-5}	0.54662×10^{-8}	0.34831×10^{-12}	0.84217×10^{-18}
100.0	0.16423×10^{-5}	0.27800×10^{-8}	0.10340×10^{-12}	0.11806×10^{-18}

$$n_a h_1^a(u)+n_b h_1^b(u)=-u^{3/2}[\psi_1^a(a)+\psi_1^b(a)]\ , \tag{51}$$

$$\tfrac{1}{2}n_a^2 h_2^a(u)+\tfrac{1}{2}n_b^2 h_2^b(u)+n_a n_b h_2^{ab}(u) =u^{3/1}[\psi_{2,\Lambda}^a(a)+\psi_{2,\Lambda}^{ab}(a)+\psi_{2,\Lambda}^b(a)]\ ,$$

for $p=1.0$

$$n_a h_1^a(u)+n_b h_1^b(u)=-u^{3/2}\psi_1^b(a)\ ,$$

$$\tfrac{1}{2}n_a^2 h_2^a(u)+\tfrac{1}{2}n_b^2 h_2^b(u)+n_a n_b h_2^{ab}(u)=u^{3/2}\psi_{2,\Lambda}^b(a)$$

TABLE II. Low-frequency component Ne proton ($p \cong 1$) at an ion Ne^{9+} immersed in a dense proton plasma.

β	V 0.2	0.4	0.6	0.8
0.1	$0.833\,16\times10^{-2}$	$0.195\,36\times10^{-1}$	$0.443\,93\times10^{-1}$	$0.947\,22\times10^{-1}$
0.2	$0.324\,59\times10^{-1}$	$0.748\,96\times10^{-1}$	0.164 83	0.331 60
0.3	$0.704\,31\times10^{-1}$	0.157 16	0.328 78	0.606 08
0.4	0.118 61	0.253 90	0.497 24	0.826 15
0.5	0.173 01	0.351 91	0.637 87	0.950 18
0.6	0.229 35	0.439 88	0.732 18	0.980 69
0.7	0.283 62	0.509 41	0.775 78	0.941 11
0.8	0.332 41	0.556 72	0.774 50	0.857 96
0.9	0.373 23	0.581 18	0.739 27	0.753 19
1.0	0.404 54	0.584 93	0.682 08	0.642 94
1.1	0.425 73	0.571 69	0.613 44	0.538 17
1.2	0.437 00	0.545 77	0.541 35	0.445 30
1.3	0.439 17	0.511 37	0.471 25	0.366 77
1.4	0.433 47	0.472 09	0.406 36	0.301 86
1.5	0.421 33	0.430 83	0.348 31	0.248 09
1.6	0.404 25	0.389 70	0.297 63	0.202 71
1.7	0.383 63	0.350 12	0.254 10	0.163 74
1.8	0.360 75	0.313 01	0.217 05	0.130 41
1.9	0.336 68	0.278 85	0.185 62	0.102 92
2.0	0.312 28	0.247 84	0.158 95	$0.816\,37\times10^{-1}$
2.5	0.203 00	0.136 96	$0.743\,78\times10^{-1}$	$0.340\,63\times10^{-1}$
3.0	0.128 93	$0.784\,34\times10^{-1}$	$0.374\,90\times10^{-1}$	$0.157\,58\times10^{-1}$
3.5	$0.842\,68\times10^{-1}$	$0.474\,18\times10^{-1}$	$0.210\,93\times10^{-1}$	$0.831\,44\times10^{-1}$
4.0	$0.569\,19\times10^{-1}$	$0.310\,60\times10^{-1}$	$0.130\,27\times10^{-1}$	$0.462\,22\times10^{-2}$
4.5	$0.399\,92\times10^{-1}$	$0.214\,71\times10^{-1}$	$0.825\,98\times10^{-2}$	$0.267\,28\times10^{-2}$
5.0	$0.293\,48\times10^{-1}$	$0.154\,15\times10^{-1}$	$0.552\,81\times10^{-2}$	$0.163\,15\times10^{-2}$
6.0	$0.169\,68\times10^{-1}$	$0.840\,66\times10^{-2}$	$0.265\,84\times10^{-2}$	$0.683\,32\times10^{-3}$
7.0	$0.106\,48\times10^{-1}$	$0.498\,03\times10^{-2}$	$0.140\,36\times10^{-2}$	$0.321\,55\times10^{-3}$
8.0	$0.711\,66\times10^{-2}$	$0.317\,89\times10^{-2}$	$0.798\,50\times10^{-3}$	$0.166\,83\times10^{-3}$
9.0	$0.500\,49\times10^{-2}$	$0.208\,84\times10^{-2}$	$0.494\,76\times10^{-3}$	$0.900\,31\times10^{-4}$
10.0	$0.363\,08\times10^{-2}$	$0.144\,54\times10^{-2}$	$0.316\,98\times10^{-3}$	$0.560\,77\times10^{-4}$
12.0	$0.201\,69\times10^{-2}$	$0.716\,75\times10^{-3}$	$0.151\,44\times10^{-3}$	$0.211\,30\times10^{-4}$
14.0	$0.133\,67\times10^{-2}$	$0.431\,05\times10^{-3}$	$0.774\,20\times10^{-4}$	$0.859\,74\times10^{-5}$
16.0	$0.933\,05\times10^{-3}$	$0.267\,23\times10^{-3}$	$0.423\,82\times10^{-4}$	$0.399\,27\times10^{-5}$
18.0	$0.679\,82\times10^{-3}$	$0.178\,50\times10^{-3}$	$0.246\,06\times10^{-4}$	$0.190\,35\times10^{-5}$
20.0	$0.497\,13\times10^{-3}$	$0.123\,12\times10^{-3}$	$0.148\,36\times10^{-4}$	$0.949\,50\times10^{-6}$
22.0	$0.385\,36\times10^{-3}$	$0.885\,09\times10^{-4}$	$0.898\,80\times10^{-5}$	$0.506\,14\times10^{-6}$
24.0	$0.302\,91\times10^{-3}$	$0.645\,98\times10^{-4}$	$0.578\,70\times10^{-5}$	$0.274\,99\times10^{-6}$
26.0	$0.242\,10\times10^{-3}$	$0.480\,59\times10^{-4}$	$0.381\,33\times10^{-5}$	$0.153\,71\times10^{-6}$
28.0	$0.197\,32\times10^{-3}$	$0.366\,03\times10^{-4}$	$0.258\,92\times10^{-5}$	$0.893\,11\times10^{-7}$
30.0	$0.164\,46\times10^{-3}$	$0.274\,95\times10^{-4}$	$0.182\,47\times10^{-5}$	$0.545\,31\times10^{-7}$
35.0	$0.104\,62\times10^{-3}$	$0.155\,02\times10^{-4}$	$0.800\,70\times10^{-5}$	$0.153\,66\times10^{-7}$
40.0	$0.711\,16\times10^{-4}$	$0.908\,82\times10^{-5}$	$0.367\,51\times10^{-6}$	$0.496\,61\times10^{-8}$
45.0	$0.506\,58\times10^{-4}$	$0.564\,29\times10^{-5}$	$0.181\,77\times10^{-6}$	$0.199\,68\times10^{-8}$
50.0	$0.367\,23\times10^{-4}$	$0.356\,72\times10^{-5}$	$0.915\,90\times10^{-7}$	$0.734\,44\times10^{-9}$
60.0	$0.217\,44\times10^{-4}$	$0.166\,59\times10^{-5}$	$0.288\,61\times10^{-7}$	$0.133\,97\times10^{-9}$
70.0	$0.141\,23\times10^{-4}$	$0.813\,97\times10^{-6}$	$0.955\,69\times10^{-8}$	$0.258\,24\times10^{-10}$
80.0	$0.931\,17\times10^{-5}$	$0.467\,10\times10^{-6}$	$0.400\,67\times10^{-8}$	$0.699\,37\times10^{-11}$
90.0	$0.627\,77\times10^{-5}$	$0.254\,14\times10^{-6}$	$0.152\,69\times10^{-8}$	$0.162\,31\times10^{-11}$
100.0	$0.464\,49\times10^{-5}$	$0.158\,40\times10^{-6}$	$0.715\,69\times10^{-9}$	$0.511\,40\times10^{-12}$

with the $\psi^{j}_{1,2}(a)$'s explained in terms of their respective $g_2(X)$ as (see Fig. 6)

$$\psi_1^a(a)\to g_2(X)=\exp\left[-Z_a^2\Lambda\frac{e^{-RX}}{X}\right],$$

$$\psi_1^b(a)\to g_2(X)=\exp\left[-Z_aZ_b\Lambda\frac{e^{-RX}}{X}\right],$$

$$\psi_2^a(a)\to g_2(X)=\exp\left[-Z_a^2\Lambda\frac{e^{-RX}}{X}\right]-1, \tag{52}$$

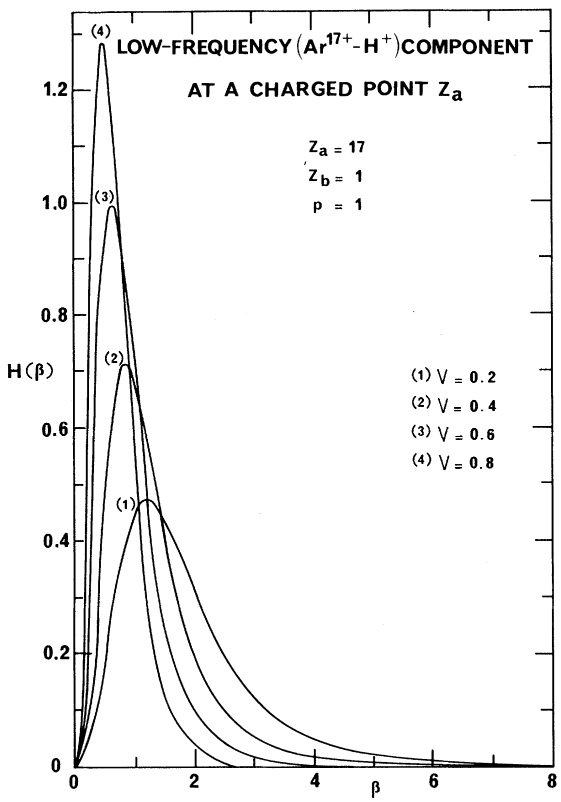

FIG. 3. Low-frequency electric microfield $H(\beta)$ values in Ar^{17+}-H^+ at $Z_a=Ar^{17+}$ for heavy impurities immersed in a dense proton fluid ($p\cong 1$).

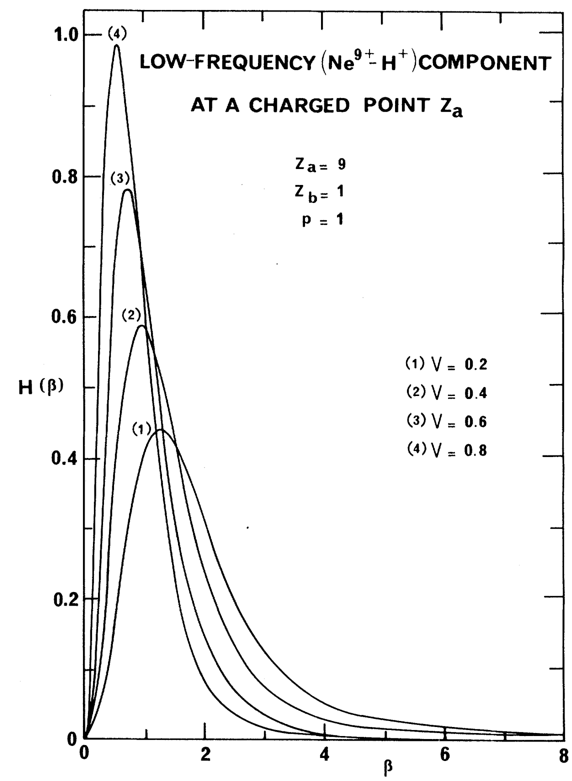

FIG. 4. Low-frequency electric microfield $H(\beta)$ values in Ne^{9+}-H^+ at $Z_a=Ne^{9+}$ for heavy impurities immersed in a dense proton fluid ($p\cong 1$).

$$\psi_2^{ab}(a)\to g_2(X)=\exp\left[-Z_aZ_b\Lambda\frac{e^{-RX}}{X}\right]-1\,,$$

$$\psi_2^{b}(ab)\to g_2(X)=\exp\left[-Z_b^2\Lambda\frac{e^{-RX}}{X}\right]-1$$

with

$$F(u)=\exp\{-u^{3/2}[\psi_c^a(a)+\psi_c^b(a)-\psi_{2,\Lambda}^a(a) \\ -\psi_{2,\Lambda}^b(a)-\psi_{2,\Lambda}^{ab}(a)]\} \tag{53}$$

and

$$\psi_c^a(a)=\frac{15}{2(2\pi)^{1/2}}\frac{(1-p)}{Z_a+p(Z_b-Z_a)}\frac{1}{a^3} \\ \times\int_0^\infty[1-j_0(Z_1^a)] \\ \times\exp\left[-Z_a^2\Lambda\frac{e^{-RX_1}}{X_1}\right]X_1^2dX_1\,,$$

$$\psi_c^b(a)=\frac{15}{2(2\pi)^{1/2}}\frac{p}{Z_a+p(Z_b-Z_a)}\frac{1}{a^3} \\ \times\int_0^\infty[1-j_0(Z_1^b)] \\ \times\exp\left[-Z_aZ_b\Lambda\frac{e^{-RX_1}}{X_1}\right]X_1^2dX_1\,, \tag{54}$$

where

$$Z_1^{a,b}=Z_{a,b}\frac{a^2}{X_1^2}(1+X_1)e^{-X_1}$$

and

$$R^2=\left[1+\frac{1}{Z_a+p(Z_b-Z_a)}\right] \\ \times\left[1+\frac{(Z_a-1)(Z_a+1)+p(Z_b-Z_a)(Z_b+Z_a)}{(Z_a+1)+p(Z_b-Z_a)}\right].$$

The resulting $H(\beta)$ are given in Table IV and Fig. 7 for $V=0.2$ (weak coupling). The variations of the overall plasma parameter Λ [cf. Eq. (5)] are explained in Fig. 7. The strongly coupled case ($V=0.8$) is numerically considered in Table V and Fig. 8.

Both Figs. 7 and 8 show clearly that it takes only a small heavy-ion proportion to switch the $H(\beta)$ distributions around the pure heavy-ion phase ($p\simeq 0$) one. Moreover, the p dependence of Λ [Eq. (5)] altogether with the Λ dependence of V [Eq. (6)] shows that proportion effects are basically monitored by the coupling parameter Λ.

It is also gratifying that the present results fall within

TABLE III. Low-frequency $H(\beta)$ in a pure Al^{10+} plasma ($p=01$).

β	V 0.2	0.4	0.6	0.8
0.1	0.20920×10^{-2}	0.56333×10^{-2}	0.20459×10^{-1}	0.81649×10^{-1}
0.2	0.82898×10^{-2}	0.21974×10^{-1}	0.74456×10^{-1}	0.23333
0.3	0.18363×10^{-1}	0.47449×10^{-1}	0.14567	0.36055
0.4	0.31940×10^{-1}	0.79754×10^{-1}	0.21849	0.44253
0.5	0.48535×10^{-1}	0.11623	0.28277	0.48581
0.6	0.67565×10^{-1}	0.15424	0.33377	0.50040
0.7	0.88387×10^{-1}	0.19145	0.37043	0.49567
0.8	0.11033	0.22601	0.39383	0.47991
0.9	0.13272	0.25663	0.40606	0.45839
1.0	0.15491	0.28257	0.40938	0.43362
1.1	0.17632	0.30350	0.40567	0.40700
1.2	0.19643	0.31946	0.39652	0.38163
1.3	0.21482	0.33071	0.38342	0.35607
1.4	0.23116	0.33765	0.36776	0.32807
1.5	0.24522	0.34074	0.35063	0.30073
1.6	0.25684	0.34044	0.33274	0.27861
1.7	0.26600	0.33722	0.31461	0.26217
1.8	0.27270	0.33150	0.29661	0.24803
1.9	0.27705	0.32367	0.27896	0.23333
2.0	0.27918	0.31411	0.26170	0.21702
2.2	0.27754	0.29114	0.22864	0.18205
2.4	0.26947	0.26508	0.19909	0.15428
2.6	0.25675	0.23804	0.17375	0.13312
2.8	0.24099	0.21164	0.15248	0.11949
3.0	0.22354	0.18697	0.13455	0.10148
3.5	0.17843	0.13568	0.10091	0.78978×10^{-1}
4.0	0.13687	0.98670×10^{-1}	0.74251×10^{-1}	0.59546×10^{-1}
4.5	0.10113	0.72869×10^{-1}	0.53986×10^{-1}	0.43348×10^{-1}
5.0	0.71614×10^{-1}	0.54222×10^{-1}	0.38580×10^{-1}	0.30641×10^{-1}
6.0	0.38426×10^{-1}	0.26840×10^{-1}	0.18316×10^{-1}	0.15654×10^{-1}
7.0	0.22764×10^{-1}	0.14440×10^{-1}	0.97108×10^{-2}	0.77737×10^{-2}
8.0	0.14699×10^{-1}	0.80775×10^{-2}	0.55243×10^{-2}	0.39109×10^{-2}
9.0	0.99860×10^{-2}	0.48350×10^{-2}	0.31217×10^{-2}	0.20625×10^{-2}
10.0	0.70711×10^{-2}	0.28239×10^{-2}	0.17454×10^{-2}	0.11860×10^{-2}
12.0	0.40419×10^{-2}	0.13279×10^{-2}	0.65487×10^{-3}	0.38285×10^{-3}
14.0	0.24213×10^{-2}	0.65620×10^{-3}	0.25215×10^{-3}	0.13906×10^{-3}
16.0	0.15559×10^{-2}	0.33354×10^{-3}	0.10690×10^{-3}	0.52259×10^{-4}
18.0	0.10507×10^{-2}	0.19282×10^{-3}	0.48883×10^{-4}	0.21750×10^{-4}
20.0	0.75731×10^{-3}	0.11054×10^{-3}	0.22666×10^{-4}	0.80130×10^{-5}
22.0	0.56214×10^{-3}	0.69958×10^{-4}	0.11474×10^{-4}	0.35967×10^{-5}
24.0	0.40984×10^{-3}	0.42723×10^{-4}	0.55827×10^{-5}	0.14819×10^{-5}
26.0	0.31735×10^{-3}	0.26588×10^{-4}	0.29445×10^{-5}	0.68092×10^{-6}
28.0	0.24550×10^{-3}	0.17003×10^{-4}	0.15213×10^{-5}	0.29159×10^{-6}
30.0	0.19710×10^{-3}	0.11024×10^{-4}	0.85678×10^{-6}	0.11546×10^{-6}
35.0	0.11370×10^{-3}	0.42436×10^{-5}	0.18889×10^{-6}	0.15430×10^{-7}
40.0	0.63591×10^{-4}	0.14200×10^{-5}	0.40307×10^{-7}	0.14747×10^{-8}
45.0	0.40693×10^{-4}	0.61569×10^{-6}	0.87516×10^{-8}	0.23055×10^{-9}
50.0	0.27898×10^{-4}	0.28075×10^{-6}	0.20601×10^{-8}	0.27650×10^{-10}
60.0	0.13074×10^{-4}	0.66907×10^{-7}	0.19622×10^{-9}	0.82026×10^{-12}
70.0	0.68839×10^{-5}	0.19039×10^{-7}	0.21296×10^{-10}	0.21135×10^{-13}
80.0	0.38032×10^{-5}	0.53058×10^{-8}	0.28575×10^{-11}	0.16464×10^{-14}
90.0	0.23853×10^{-5}	0.16797×10^{-8}	0.36045×10^{-12}	0.65886×10^{-16}
100.0	0.14822×10^{-5}	0.64901×10^{-9}	0.56400×10^{-13}	0.29368×10^{-17}

0.5% of the TH ones,[2] which demonstrates the efficiency of the much shorter BM code. Obviously, Ar^{17+}-H^{+} mixtures display very similar trends. Thus we do not need to detail here the corresponding data.

VI. Ar-Ne MIXTURES

With a heavy-ion fusion perspective, we think it rather instructive to move to Ar^{17+}-Ne^{9+} mixtures in various

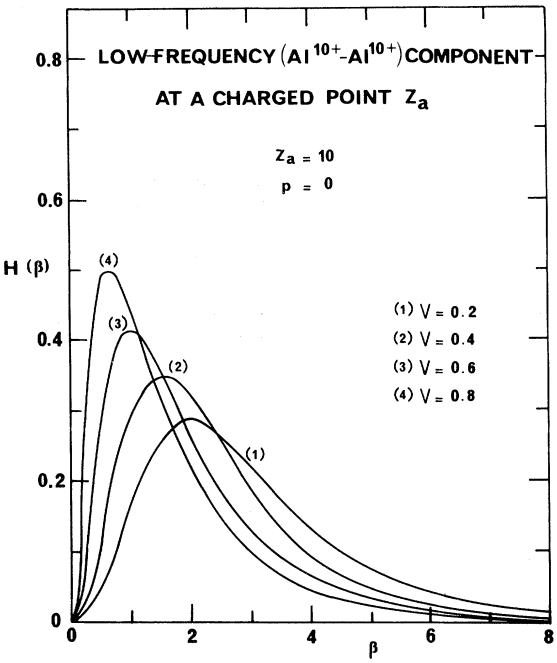

FIG. 5. Low-frequency $H(\beta)$ in a pure Al^{10+} phase.

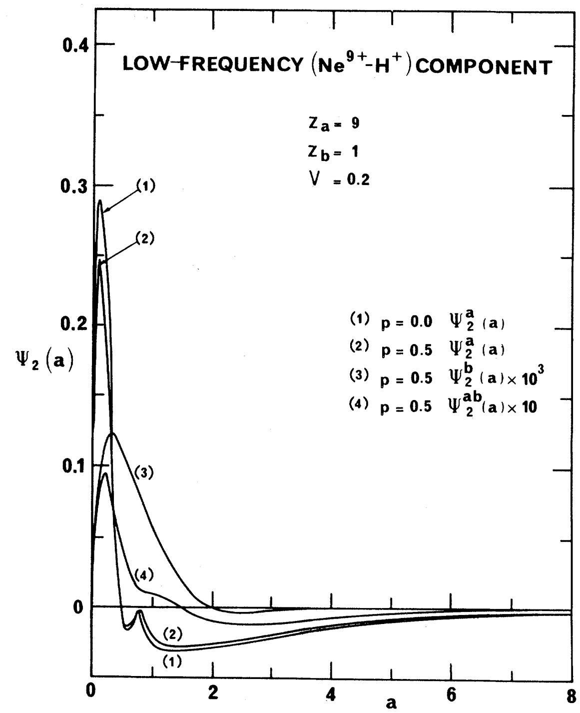

FIG. 6. $\psi_2(a)$ [Eq. (52)] plotted for $V=0.2$ and a Ne^{9+}-H^+ mixture.

relative proportions, and compute the distributions $H(\beta)$ at a Ne^{9+} and Ar^{17+} emitter, respectively. Table VI together with Fig. 9, display the given $H(\beta)$ at a Z_a charge for $V=0.2$ and $p=0.5$, so that everything else remains unchanged; the charge of the tagged emitter is seen to play an important role, especially at the peak values (Fig. 9). As before the asymptotic $H(\beta)$ with $\beta>5$ are deduced from the nearest-neighbor approximation (NNA) worked out in Sec. VII. The present results together with those obtained in the preceding section show us that the low-frequency microfield distributions are mostly dependent on Λ and Z_a in BIM.

VII. $H(\beta)$ WITH LARGE-β VALUES

The BM scheme worked out successfully in Sec. II is mostly accurate in the $0\le\beta\le4.5$ range (first column of the calculated data). In contradistinction to the neutral- or single-ionized emitter, the large $Z_a \gg 1$ considered here precludes any smooth asymptotic extrapolation for $\beta>5$. The usual standard techniques would produce too many spurious oscillations. This explains why one has to switch gear toward other numerical procedures based on the NNA.

A. Nearest-neighbor approximation

For this purpose, let us consider a sphere located at the origin (emitter). The probability of finding a given particle between 0 and r is then

$$p(r)+p'(r)=1\ , \tag{55}$$

where $p'(r)$ denotes a probability for finding no particles between 0 and r. It obviously fulfills

$$p'(r+dr)=p'(r)p'(dr)\ . \tag{56}$$

Denoting again as $p\,dr$ the probability of finding a particle between r and $r+dr$, which obeys

$$p'(dr)+p\,dr=1\ , \tag{57}$$

and

$$p'(r+dr)=p'(r)(1-p\,dr)\ ,$$

so that

$$p'(r)=\exp\left[-\int_0^r p\,dr'\right]\ , \tag{58}$$

where $p'(r=0)=1$, one finally obtains

$$p(r)=1-\exp\left[-\int_0^r p\,dr'\right]\ . \tag{59}$$

From the last two equations, one deduces immediately $(dp+dp'=0)$

$$dp=p\,dr\exp\left[-\int_0^r p\,dr'\right]\ . \tag{60}$$

Therefore, the probability for finding a β value at the origin is equal to the probability of finding a charged particle located at r from the origin, so that

$$H(\beta)d\beta=dp\ . \tag{61}$$

In order to continue further, let us notice that

$$p\,dr=N\frac{4\pi r^2}{V}g_2(r)dr\ , \tag{62}$$

TABLE IV. Low-frequency $H(\beta)$ in a Ne^{9+}-H^{+} mixture ($V=0.2$) at a neon point for various proportions.

β	P 1.0	0.5	0.0
0.1	$0.833\,16\times10^{-2}$	$0.246\,55\times10^{-2}$	$0.220\,37\times10^{-2}$
0.2	$0.325\,49\times10^{-1}$	$0.975\,84\times10^{-2}$	$0.872\,89\times10^{-2}$
0.3	$0.704\,32\times10^{-1}$	$0.215\,75\times10^{-1}$	$0.193\,23\times10^{-1}$
0.4	0.118 61	$0.374\,32\times10^{-1}$	$0.335\,83\times10^{-1}$
0.5	0.173 01	$0.566\,93\times10^{-1}$	0.50975×10^{-1}
0.6	0.229 35	$0.786\,10\times10^{-1}$	$0.708\,68\times10^{-1}$
0.7	0.283 62	0.102 37	$0.925\,67\times10^{-1}$
0.8	0.332 41	0.127 12	0.115 35
0.9	0.373 23	0.152 05	0.148 49
1.0	0.404 54	0.176 37	0.161 30
1.1	0.425 73	0.199 42	0.18318
1.2	0.437 00	0.220 61	0.203 59
1.3	0.439 17	0.239 49	0.222 09
1.4	0.433 47	0.255 74	0.238 35
1.5	0.421 33	0.269 14	0.252 14
1.6	0.404 25	0.279 62	0.263 35
1.7	0.383 63	0.287 19	0.271 93
1.8	0.360 75	0.291 94	0.277 95
1.9	0.336 68	0.294 06	0.281 52
2.0	0.312 28	0.293 76	0.282 79
2.5	0.203 00	0.265 36	0.262 70
3.0	0.128 93	0.215 40	0.219 13
3.5	$0.842\,68\times10^{-1}$	0.165 19	0.172 22
4.0	$0.569\,19\times10^{-1}$	0.122 69	0.130 48
4.5	$0.399\,92\times10^{-1}$	$0.885\,96\times10^{-1}$	$0.957\,10\times10^{-1}$
5.0	$0.293\,48\times10^{-1}$	$0.619\,41\times10^{-1}$	$0.677\,63\times10^{-1}$
6.0	$0.169\,68\times10^{-1}$	$0.342\,47\times10^{-1}$	$0.375\,51\times10^{-1}$
7.0	$0.106\,48\times10^{-1}$	$0.207\,61\times10^{-1}$	$0.227\,64\times10^{-1}$
8.0	$0.711\,66\times10^{-2}$	$0.134\,05\times10^{-1}$	$0.145\,30\times10^{-1}$
9.0	$0.500\,49\times10^{-2}$	$0.921\,28\times10^{-2}$	$0.987\,17\times10^{-2}$
10.0	$0.363\,08\times10^{-2}$	$0.650\,92\times10^{-2}$	$0.695\,81\times10^{-2}$
12.0	$0.201\,69\times10^{-2}$	$0.365\,80\times10^{-2}$	$0.389\,64\times10^{-2}$
14.0	$0.133\,67\times10^{-2}$	$0.232\,84\times10^{-2}$	$0.247\,54\times10^{-2}$
16.0	$0.933\,05\times10^{-3}$	$0.161\,01\times10^{-2}$	$0.171\,15\times10^{-2}$
18.0	$0.679\,82\times10^{-3}$	$0.113\,43\times10^{-2}$	$0.120\,36\times10^{-2}$
20.0	$0.497\,13\times10^{-3}$	$0.780\,17\times10^{-3}$	$0.824\,77\times10^{-3}$
22.0	$0.385\,36\times10^{-3}$	$0.606\,63\times10^{-3}$	$0.641\,62\times10^{-3}$
24.0	$0.302\,81\times10^{-3}$	$0.443\,46\times10^{-3}$	$0.466\,71\times10^{-3}$
26.0	$0.242\,10\times10^{-3}$	$0.354\,55\times10^{-3}$	$0.373\,23\times10^{-3}$
28.0	$0.197\,32\times10^{-3}$	$0.266\,04\times10^{-3}$	$0.278\,31\times10^{-3}$
30.0	$0.164\,46\times10^{-3}$	$0.208\,82\times10^{-3}$	$0.217\,38\times10^{-3}$
35.0	$0.104\,62\times10^{-3}$	$0.123\,49\times10^{-3}$	$0.127\,74\times10^{-3}$
40.0	$0.711\,16\times10^{-4}$	$0.748\,07\times10^{-4}$	$0.765\,07\times10^{-4}$
45.0	$0.506\,58\times10^{-4}$	$0.505\,18\times10^{-4}$	$0.513\,73\times10^{-4}$
50.0	$0.367\,23\times10^{-4}$	$0.332\,61\times10^{-4}$	$0.334\,37\times10^{-4}$
60.0	$0.217\,44\times10^{-4}$	$0.174\,25\times10^{-4}$	$0.172\,29\times10^{-4}$
70.0	$0.141\,23\times10^{-4}$	$0.104\,23\times10^{-4}$	$0.101\,17\times10^{-4}$
80.0	$0.931\,17\times10^{-5}$	$0.662\,51\times10^{-5}$	$0.643\,16\times10^{-5}$
90.0	$0.627\,77\times10^{-5}$	$0.408\,83\times10^{-5}$	$0.390\,72\times10^{-5}$
100.0	$0.464\,49\times10^{-5}$	$0.247\,53\times10^{-5}$	$0.226\,67\times10^{-5}$

in a medium containing N particles. Introducing

$$p\,dr = 4\pi r^2 n g(r)\,dr, \quad n = \frac{N}{V} \tag{63}$$

in Eq. (60) yields

$$dP = 4\pi r^2 n g(r) dr \exp\left[-\int 4\pi r'^2 n g(r') dr'\right], \tag{64}$$

when $\beta \gg 1$, the nearest neighbor is very close to the emitter, and

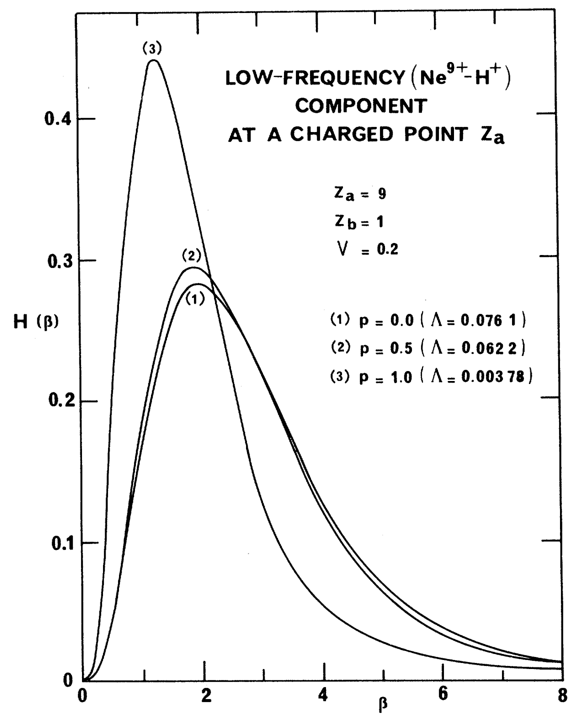

FIG. 7. Low-frequency $H(\beta)$ in Ne^{9+}-H^+ mixtures in various proportions. Weak coupling ($V=0.2$).

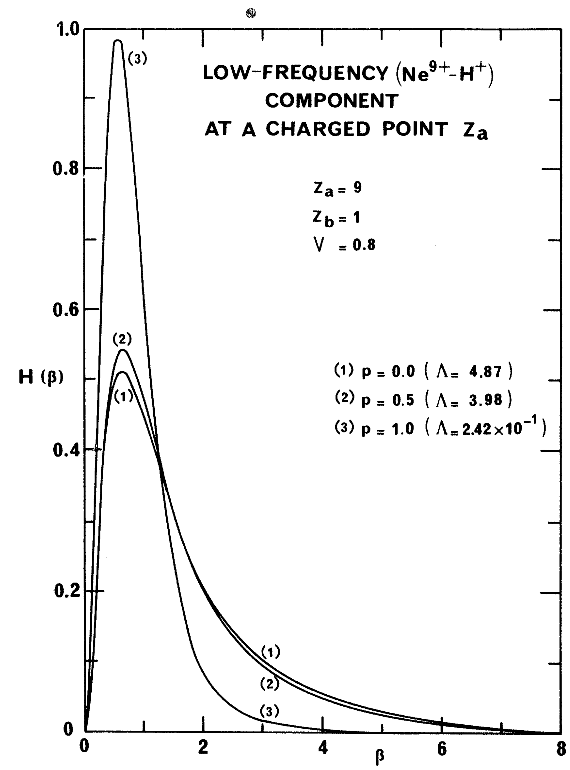

FIG. 8. Low-frequency $H(\beta)$ in Ne^{9+}-H^+ mixtures in various proportions. Strong coupling ($V=0.8$).

$$\int_0^r 4\pi r'^2 n g_2(r')dr' \ll 1 \ , \tag{65}$$

while ($n=N/V$)

$$dP \sim 4\pi r^2 n g(r) dr \ . \tag{66}$$

Recalling that $V=r_0/\lambda_{D_e}$ and $x=r/\lambda_{D_e}$ while setting $\xi=r/r_0$ and altogether collecting Eqs. (61) and (64), one gets

$$H(\beta)d\beta = \frac{15}{2(2\pi)^{1/2}}\frac{n}{n_e}g(X)\xi^2 d\xi \times \exp\left[-\int_0^{\xi}\frac{15}{2(2\pi)^{1/2}}\frac{n}{n_e}g(X')\xi'^2 d\xi'\right] \tag{67}$$

which will be discussed later on.

B. High frequency

Recalling that $E_0=e/r_0^2$ and $\beta=E/E_0$, one also obtains $\beta=1/\xi^2$. Introducing $n=n_e$, Eq. (67) specializes to

$$H(\beta) = \frac{15}{4(2\pi)^{1/2}}g(X)\xi^5 \times \exp\left[-\int_0^{\xi}\frac{15}{2(2\pi)^{1/2}}g(X')\xi'^2 d\xi'\right] \tag{68}$$

with the large $\beta(\xi \to 0)$ limit

$$H(\beta) \sim \frac{15}{4(2\pi)^{1/2}}g(X)\frac{1}{\beta^{5/2}} \ . \tag{69}$$

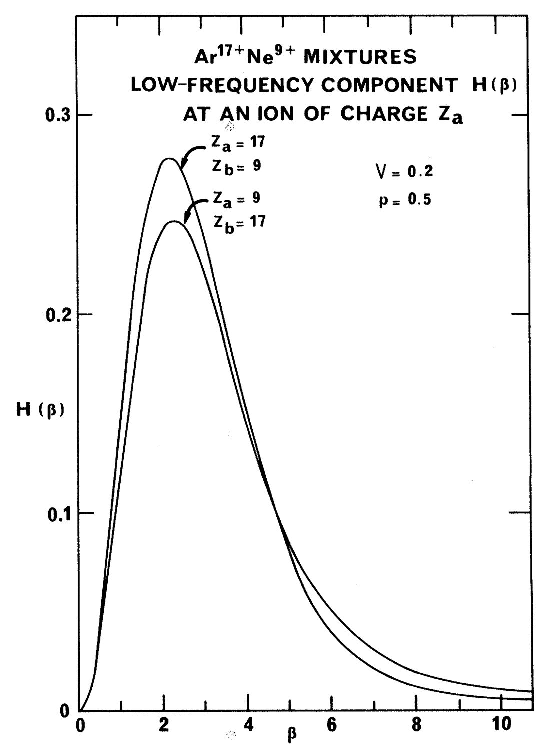

FIG. 9. Low-frequency $H(\beta)$ in Ar^{17+}-Ne^{9+} mixtures for $V=0.2$ and $p=0.5$. Emitter charge (Z_a) effect.

TABLE V. Low-frequency $H(\beta)$ at a Ne^{9+} charge in a strongly correlated Ne^{9+}-H^{+} mixture ($V=0.8$).

		P	
β	1.0	0.5	0.0
0.1	0.94722×10^{-1}	0.70390×10^{-1}	0.75533×10^{-1}
0.2	0.331 60	0.218 67	0.222 95
0.3	0.606 08	0.359 19	0.352 83
0.4	0.826 15	0.458 32	0.439 76
0.5	0.950 18	0.514 97	0.487 64
0.6	0.980 69	0.537 79	0.506 34
0.7	0.941 11	0.536 79	0.505 16
0.8	0.857 96	0.521 11	0.491 60
0.9	0.753 19	0.497 21	0.470 78
1.0	0.642 94	0.468 69	0.445 80
1.1	0.538 17	0.437 93	0.418 70
1.2	0.445 30	0.407 14	0.392 09
1.3	0.366 77	0.376 35	0.365 00
1.4	0.301 86	0.345 01	0.335 92
1.5	0.248 09	0.314 97	0.307 53
1.6	0.202 1	0.288 95	0.283 77
1.7	0.163 74	0.267 40	0.265 34
1.8	0.130 41	0.248 53	0.249 61
1.9	0.102 92	0.230 57	0.233 92
2.0	0.81637×10^{-1}	0.212 69	0.217 14
2.5	0.34063×10^{-1}	0.137 64	0.144 83
3.0	0.15758×10^{-1}	0.94379×10^{-1}	0.99970×10^{-1}
3.5	0.83144×10^{-2}	0.68662×10^{-1}	0.72642×10^{-1}
4.0	0.46222×10^{-2}	0.49528×10^{-1}	0.52465×10^{-1}
4.5	0.26628×10^{-2}	0.34422×10^{-1}	0.39431×10^{-1}
5.0	0.16315×10^{-2}	0.23582×10^{-1}	0.29427×10^{-1}
6.0	0.68332×10^{-3}	0.10830×10^{-1}	0.14277×10^{-1}
7.0	0.32155×10^{-3}	0.54608×10^{-2}	0.70755×10^{-2}
8.0	0.16683×10^{-3}	0.28992×10^{-2}	0.36921×10^{-2}
9.0	0.90031×10^{-4}	0.15290×10^{-2}	0.20040×10^{-2}
10.0	0.56077×10^{-4}	0.85114×10^{-3}	0.11548×10^{-2}
12.0	0.21130×10^{-4}	0.28275×10^{-3}	0.38723×10^{-3}
14.0	0.85974×10^{-5}	0.99712×10^{-4}	0.14041×10^{-3}
16.0	0.39927×10^{-5}	0.38494×10^{-4}	0.55311×10^{-4}
18.0	0.19036×10^{-5}	0.15082×10^{-4}	0.22000×10^{-4}
20.0	0.94950×10^{-6}	0.60523×10^{-5}	0.88966×10^{-5}
22.0	0.50614×10^{-6}	0.25761×10^{-5}	0.37804×10^{-5}
24.0	0.27499×10^{-6}	0.11215×10^{-5}	0.16276×10^{-5}
26.0	0.15371×10^{-6}	0.49265×10^{-6}	0.69564×10^{-6}
28.0	0.89311×10^{-7}	0.23026×10^{-6}	0.31204×10^{-6}
30.0	0.54531×10^{-7}	0.10917×10^{-6}	0.13683×10^{-6}
35.0	0.15366×10^{-7}	0.20365×10^{-7}	0.19947×10^{-7}
40.0	0.49661×10^{-8}	0.49021×10^{-8}	0.31830×10^{-8}
45.0	0.19968×10^{-8}	0.16248×10^{-8}	0.54801×10^{-9}
50.0	0.73444×10^{-9}	0.56145×10^{-9}	0.10307×10^{-9}
60.0	0.13397×10^{-9}	0.99216×10^{-10}	0.39383×10^{-11}
70.0	0.25824×10^{-10}	0.19531×10^{-10}	0.16846×10^{-12}
80.0	0.69937×10^{-11}	0.54075×10^{-11}	0.92374×10^{-14}
90.0	0.16231×10^{-11}	0.12866×10^{-11}	0.60978×10^{-15}
100.0	0.51140×10^{-12}	0.41282×10^{-12}	0.39974×10^{-16}

Therefore, at a neutral point $[g(X)=1]$ one gets

$$H(\beta)\sim\frac{15}{4(2\pi)^{1/2}}\frac{1}{\beta^{5/2}}\,, \tag{70}$$

while at a single charged one $(g(X)=\exp[-\Lambda_e(e^{-X}/X)])$

$$H(\beta)\sim\frac{15}{4(2\pi)^{1/2}}\frac{1}{\beta^{5/2}}\times\exp\left[-\frac{2(2\pi)^{1/2}}{15}V^2\beta^{1/2}e^{-V/\beta^{1/2}}\right], \tag{71}$$

TABLE VI. Low-frequency $H(\beta)$ in Ar^{17+}-Ne^{9+} mixtures with $V=0.2$ and $p=0.5$.

β	$H(\beta)$	β	$H(\beta)$	β	$H(\beta)$
			Tagged emitter Ne^{9+}		
0	0.0	2.0	0.239 98	12.0	$0.530\,63\times10^{-2}$
0.1	$0.249\,62\times10^{-2}$	2.1	0.243 73	14.0	$0.330\,33\times10^{-2}$
0.2	$0.593\,84\times10^{-2}$	2.2	0.245 93	16.0	$0.216\,77\times10^{-2}$
0.3	$0.131\,90\times10^{-1}$	2.3	0.246 69	18.0	$0.148\,24\times10^{-2}$
0.4	$0.230\,29\times10^{-1}$	2.4	0.246 11	20.0	$0.104\,81\times10^{-2}$
0.5	$0.351\,63\times10^{-1}$	2.5	0.244 33	22.0	$0.761\,53\times10^{-3}$
0.6	$0.492\,37\times10^{-1}$	2.6	0.241 49	24.0	$0.566\,17\times10^{-3}$
0.7	$0.648\,54\times10^{-1}$	2.7	0.237 71	26.0	$0.429\,24\times10^{-3}$
0.8	$0.815\,88\times10^{-1}$	2.8	0.233 13	28.0	$0.330\,95\times10^{-3}$
0.9	$0.990\,06\times10^{-1}$	2.9	0.227 86	30.0	$0.258\,95\times10^{-3}$
1.0	0.116 68	3.0	0.222 03	35.0	$0.147\,93\times10^{-3}$
1.1	0.134 20	3.5	0.187 79	40.0	$0.898\,47\times10^{-4}$
1.2	0.151 20	4.0	0.151 22	45.0	$0.572\,41\times10^{-4}$
1.3	0.167 35	4.5	0.117 09	50.0	$0.378\,96\times10^{-4}$
1.4	0.182 37	5.0	$0.875\,68\times10^{-1}$	60.0	$0.181\,70\times10^{-4}$
1.5	0.196 04	6.0	$0.501\,19\times10^{-1}$	70.0	$0.954\,48\times10^{-5}$
1.6	0.208 19	7.0	$0.302\,00\times10^{-1}$	80.0	$0.537\,01\times10^{-5}$
1.7	0.218 69	8.0	$0.194\,98\times10^{-1}$	90.0	$0.318\,80\times10^{-5}$
1.8	0.227 50	9.0	$0.133\,35\times10^{-1}$	100.0	$0.197\,63\times10^{-5}$
1.9	0.234 59	10.0	$0.923\,98\times10^{-2}$		
			Tagged emitter Ar^{17+}		
0	0.0	2.0	0.274 16	12.0	$0.292\,89\times10^{-2}$
0.1	$0.178\,87\times10^{-2}$	2.1	0.277 23	14.0	$0.166\,46\times10^{-2}$
0.2	$0.709\,67\times10^{-2}$	2.2	0.278 46	16.0	$0.100\,22\times10^{-2}$
0.3	$0.157\,53\times10^{-1}$	2.3	0.278 01	18.0	$0.631\,49\times10^{-3}$
0.4	$0.274\,82\times10^{-1}$	2.4	0.276 03	20.0	$0.412\,85\times10^{-3}$
0.5	$0.419\,18\times10^{-1}$	2.5	0.272 70	22.0	$0.278\,29\times10^{-3}$
0.6	$0.586\,20\times10^{-1}$	2.6	0.268 19	24.0	$0.192\,49\times10^{-3}$
0.7	$0.770\,94\times10^{-1}$	2.7	0.262 66	26.0	$0.136\,13\times10^{-3}$
0.8	$0.968\,16\times10^{-1}$	2.8	0.256 28	28.0	$0.981\,36\times10^{-4}$
0.9	0.117 25	2.9	0.249 21	30.0	$0.719\,49\times10^{-4}$
1.0	0.137 88	3.0	0.241 57	35.0	$0.352\,25\times10^{-4}$
1.1	0.158 20	3.5	0.198 98	40.0	$0.185\,25\times10^{-4}$
1.2	0.177 76	4.0	0.155 70	45.0	$0.103\,08\times10^{-4}$
1.3	0.196 19	4.5	0.116 19	50.0	$0.600\,58\times10^{-5}$
1.4	0.213 13	5.0	$0.822\,62\times10^{-1}$	60.0	$0.227\,27\times10^{-5}$
1.5	0.228 35	6.0	$0.398\,11\times10^{-1}$	70.0	$0.962\,40\times10^{-6}$
1.6	0.241 65	7.0	$0.208\,93\times10^{-1}$	80.0	$0.443\,58\times10^{-6}$
1.7	0.252 91	8.0	$0.125\,89\times10^{-1}$	90.0	$0.218\,87\times10^{-6}$
1.8	0.262 07	9.0	$0.831\,76\times10^{-2}$	100.0	$0.114\,12\times10^{-6}$
1.9	0.269 14	10.0	$0.555\,88\times10^{-2}$		

in terms of

$$\Lambda_e=\frac{2(2\pi)^{1/2}}{15}V^3 .$$

Equation (71) yields Eq. (70) in the $V\to0$ limit.

C. Low frequency

Now the ion microfield is screened by the background electrons so that $\beta=(Z/\xi^2)(1+\xi V)e^{-\xi V}$. The corresponding asymptotic $H(\beta)$ ($\xi\to0$) thus is written

$$H(\beta)\sim\frac{15}{4(2\pi)^{1/2}}\frac{n}{n_e}\frac{\xi^5}{Z}\frac{e^{\xi V}}{\left[1+\xi V+\frac{\xi^2V^2}{2}\right]}g_2(X) \qquad (68')$$

which reduces to

$$H(\beta)\sim\frac{15}{4(2\pi)^{1/2}}\frac{n}{n_e}\frac{\xi^5}{Z} , \qquad (68'')$$

at a neutral point, while at a charged point Z_a, with

$$g_2(X)=\exp\left[-Z_aZ_b\Lambda_e\frac{e^{-RX}}{X}\right] ,$$

one gets

$$H(\beta)=H_{aa}(\beta)+H_{ab}(\beta) , \qquad (68''')$$

with

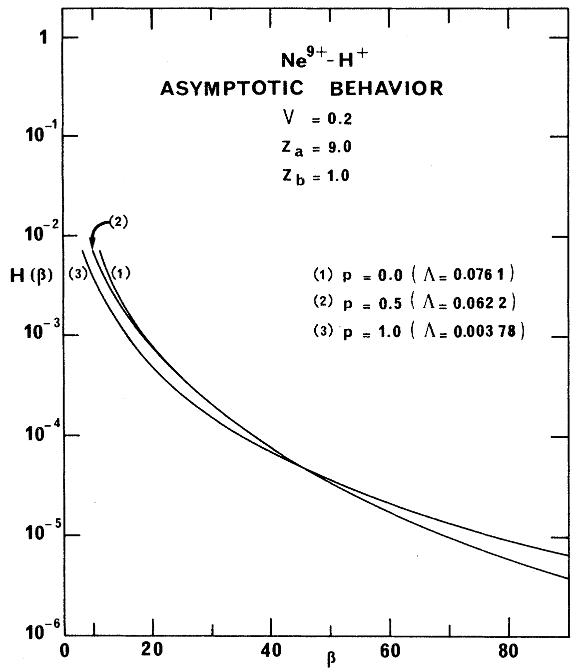

FIG. 10 Asymptotic (large β) $H(\beta)$ in Ne^{9+}-H^+ mixtures with any proportions. Weak coupling case.

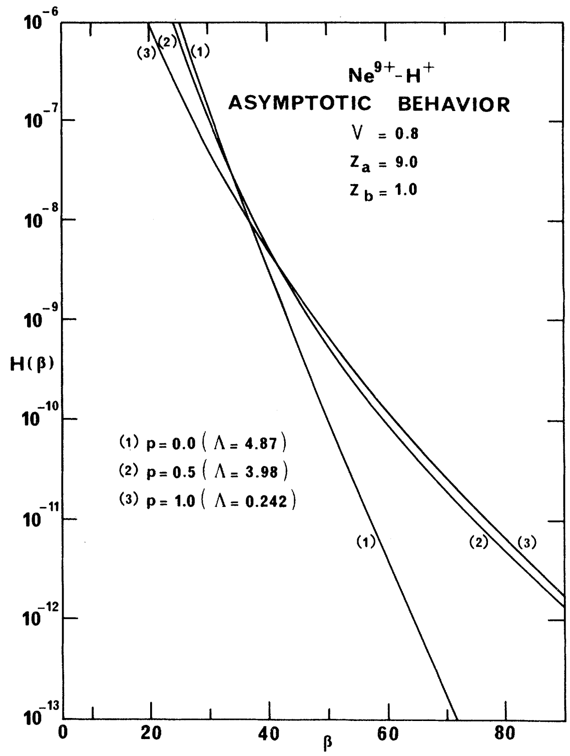

FIG. 11. Asymptotic (large β) in Ne^{9+}-H^+ mixtures with any proportions. Strong coupling cases.

$$H_{aa}(\beta)\sim\frac{15}{4(2\pi)^{1/2}}\frac{n_a}{n_e}\frac{\xi^5}{Z_a}\frac{e^{\xi V}}{\left[1+\xi V+\frac{\xi^2V^2}{2}\right]}\times\exp\left[-\frac{2(2\pi)^{1/2}}{15}V^2Z_a^2\frac{e^{-R\xi V}}{\xi}\right],$$

where

$$\beta=\frac{Z_a}{\xi^2}(1+\xi V)e^{-\xi V}, \tag{69a}$$

and also

$$H_{ab}(\xi)\simeq\frac{15}{4(2\pi)^{1/2}}\frac{n_b}{n_e}\frac{\xi^5}{Z_b}\frac{e^{\xi V}}{\left[1+\xi V+\frac{\xi^2V^2}{2}\right]}\times\exp\left[-\frac{2(2\pi)^{1/2}}{15}V^2Z_aZ_b\frac{e^{-R\xi V}}{\xi}\right],$$

where

$$\beta=\frac{Z_b}{\xi^2}(1+\xi V)e^{-\xi V}. \tag{69b}$$

In the $\beta\to\infty$ limit, for $0\le V\le 0.8$ ($\xi V\ll 1$), the asymptotic low-frequency distribution in a BIM is finally deduced from Eq. (68‴) and

$$H_{aa}(\beta)\sim\frac{15}{4(2\pi)^{1/2}}\frac{(1-p)}{Z_a+p(Z_b-Z_a)}\frac{1}{Z_a}\frac{1}{\left[\frac{\beta}{Z_a}+\frac{V^2}{2}\right]^{5/2}}\times\exp\left[-\frac{2(2\pi)^{1/2}}{15}V^2Z_a^2\left[\frac{\beta}{Z_a}+\frac{V^2}{2}\right]^{1/2}\exp\left[-\frac{RV}{\left[\frac{\beta}{Z_a}+\frac{V^2}{2}\right]^{1/2}}\right]\right], \tag{70'}$$

$$H_{ab}(\beta)\sim\frac{15}{4(2\pi)^{1/2}}\frac{p}{Z_a+p(Z_b-Z_a)}\frac{1}{Z_b}\frac{1}{\left[\frac{\beta}{Z_b}+\frac{V^2}{2}\right]^{5/2}}$$
$$\times\exp\left[-\frac{2(2\pi)^{1/2}}{15}V^2Z_aZ_b\left[\frac{\beta}{Z_b}+\frac{V^2}{2}\right]^{1/2}\exp\left[-\frac{RV}{\left[\frac{\beta}{Z_b}+\frac{V^2}{2}\right]^{1/2}}\right]\right]. \tag{70''}$$

D. Numerical results

Equations (70′) and (70″) have already been used to compute the low frequency $H(\beta)$'s in Tables I–IV for $\beta\geq 5$.

The most salient feature of the present asymptotic calculations is afforded by the equal proportion curve $p=0.5$ switching over from $p=0$ at weak coupling (Fig. 10 with $V=0.2$) to $p=1$ at large coupling (Fig. 11 with $V=0.8$). This versatile behavior is mostly based on the observation that a large Z_a emitter will tend to repel other Z_a perturbers, so that lighter ones (protons) will get closer to it.

A last interesting result concerns the extreme asymptotic limit

$$\frac{\beta}{Z_a}\gg\frac{V^2}{2}, \tag{72}$$

with

$$e^{-RVZ_a^{1/2}/\beta^{1/2}}\sim 1,$$

where Eqs. (70′) and (70″) boil down to ($\beta>100$)

$$H(\beta)\sim\frac{15}{4(2\pi)^{1/2}}\left[\frac{1-p}{Z_a+p(Z_b-Z_a)}\right]\frac{Z_a^{3/2}}{\beta^{5/2}}\exp\left[-\frac{2(2\pi)^{1/2}}{15}Z_a^{3/2}V^2\beta^{1/2}\right]$$
$$\times\left\{1+\left[\frac{p}{1-p}\right]\left[\frac{Z_b}{Z_a}\right]^{3/2}\exp\left[\frac{2(2\pi)^{1/2}}{15}Z_a^{3/2}\left[1-\frac{Z_b^{1/2}}{Z_a^{1/2}}\right]V^2\beta^{1/2}\right]\right\} \tag{73}$$

so that

$$H(\beta)\sim H(\beta)_{a-a}\ \text{for}\ Z_a<Z_b$$

and

$$H(\beta)\sim H(\beta)_{a-b}\ \text{for}\ Z_a>Z_b\ .$$

[1]G. Bekefi, C. Deutsch, and B. Ya'akobi, in *Laser Plasmas*, edited by G. Bekefi (Wiley, New York, 1976), Chap. 13.
[2]R. J. Tighe and C. F. Hooper, Jr., Phys. Rev. A 14, 1514 (1976); 15, 1773 (1977); 17, 410 (1978) (hereafter referred to as TH).
[3]B. Held, C. Deutsch, and M.-M. Gombert, Phys. Rev. A 29, 896 (1984), following paper.
[4]H. R. Griem, *Spectral Line Broadening by Plasmas* (Academic, New York, 1974).
[5]M. Baranger and B. Mozer, Phys. Rev. 115, 521 (1959); 118, 626 (1960).
[6]B. Held and C. Deutsch, Phys. Rev. A 24, 540 (1981).
[7]C. F. Hooper, Jr., Phys. Rev. 149, 77 (1966); 165, 215 (1968).
[8]C. Deutsch, Y. Furutani, and M. M. Gombert, Phys. Rev. A 13, 2244 (1976); Phys. Rep. 69, 85 (1981).
[9]B. Ya'akobi *et al.*, Phys. Rev. A 19, 1247 (1979).
[10]See, for instance, the Proceedings of the Darmstadt Symposium on Accelerator Aspects of Heavy Ion Fusion, Gesellschaft für Schwerionenforschung, Darmstadt, April 1982 (unpublished).